Earth and Planetary Science Letters, 119 (1993) 71–83
Elsevier Science Publishers B.V., Amsterdam

[MK]

Highly permeable and layered Jurassic oceanic crust in the western Pacific

Roger L. Larson [a], Andrew T. Fisher [b], Richard D. Jarrard [c], Keir Becker [d] and Ocean Drilling Program Leg 144 Shipboard Scientific Party [1]

[a] *Graduate School of Oceanography, University of Rhode Island, Narragansett, RI 02882, USA*
[b] *Department of Geophysics and Ocean Drilling Program, Texas A&M University, College Station, TX 77843, USA*
[c] *Department of Geology and Geophysics, University of Utah, Salt Lake City, UT 84112, USA*
[d] *Rosenstiel School of Marine and Atmospheric Sciences, University of Miami, 4600 Rickenbacker Causeway, Miami, FL 33149, USA*

Received March 15, 1993; revision accepted June 20, 1993

ABSTRACT

Bulk permeability was determined from drillstring packer measurements in ODP Hole 801C in Jurassic oceanic crust in the western Pacific. The values average 8×10^{-14} m^2 over 93 m of open hole, or 4×10^{-13} m^2 if the permeable interval is confined to an 18 m thick hydrothermal zone within oceanic basement. These values are about 1–10 times higher than those reported for the upper sections of Holes 395A, 504B and 735B in 3.7, 5.9 and 11 Ma old oceanic crust respectively. The discovery that 160 Ma old oceanic crust contains a zone with extremely high permeability is not predicted by any model of ocean crustal evolution. The high permeability interval appears to be associated with the burial by off-ridge volcanism of a zone of hydrothermal precipitates and altered basalts. The generality of this result may depend on the generality of off-ridge volcanism necessary to create and preserve such zones of high permeability within the ocean crustal section. Although the crustal and permeability structures detected at Hole 801C may not fit easily into currently accepted models of crustal accretion and aging, the generality of off-ridge volcanism suggests that these structures could actually be typical of large portions of the world's oceanic crust.

1. Geological background

Ocean Drilling Program (ODP) Hole 801C was drilled through sediments and into oceanic crust of Middle Jurassic age (160 Ma) at 18°38.5′N, 156°21.6′E in the Pigafetta Basin of the western Pacific Ocean (Fig. 1) during ODP Leg 129 [1]. This is a drillhole into the world's oldest *in-situ* oceanic crust [2–4]. Because of its extreme age, all models for the physical evolution of oceanic crust predict that it would have an extremely low porosity (and by inference, low bulk permeability), although no measurements of bulk permeability had been made in *in-situ* oceanic crust older than 11 Ma. We designed a comprehensive set of logging and permeability measurements for Hole 801C in order to provide an end-member characterization of very old oceanic crust formed by rapid seafloor spreading. These measurements were conducted after reentry into Hole 801C during Leg 144 [5]. We successfully logged most of the exposed basement at the bottom of the hole below the caving pipe with geophysical, geochemical, formation microscanner, temperature and magnetometer tools, and then conducted permeability experiments. Our most surprising result was the permeability determination, which we report here in detail using some of the geophysical logs and the temperature log as ancillary information.

[1] A. Arnaud-Vanneau, D.D. Bergersen, Y. Bogdanov, H.W. Bohrmann, B. Buchardt, G. Camoin, D.M. Christie, J.J. Dieu, P. Enos, E. Erba, J. Fenner, J.S. Gee, J.A. Haggerty, M.J. Head, P.R.N. Hobbs, H. Ito, L. Jansa, J.W. Ladd, J.M. Lincoln, M. Nakanishi, J.G. Ogg, B.N. Opdyke, P.N. Pearson, I. Premoli Silva, T.M. Quinn, F.R. Rack, D.K. Watkins and P.A. Wilson

2. Geophysical logging results

Hole 801C was first logged with a geophysical combination string, consisting of natural gamma, lithodensity, neutron porosity, long-spaced sonic, and temperature tools (Fig. 2). Temperature data from this first logging run indicate that the thermal regime in Hole 801C is dominantly conductive. The water in the borehole appears to have thermally equilibrated with the surrounding formation in the 2.5 yr since the hole was drilled.

The geophysical logs of Leg 144 confirmed the general three-layer stratigraphy determined by coring on Leg 129 (Fig. 2). The open portion of the hole below 480 m below seafloor (mbsf) consists of alkali basalts from 480 to 510 mbsf, a hydrothermal zone of chemical precipitate and altered alkali basalts from 510 to 528 mbsf, and tholeiitic basalts from 528 mbsf to the bottom of the hole at 594 mbsf. The alkali basalts are 4–14 Ma younger than the tholeiitic basalts, and thus

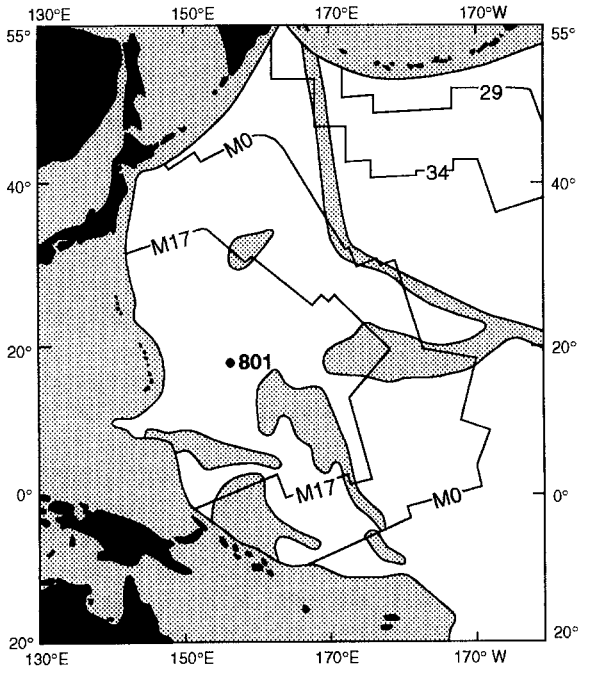

Fig. 1. Location of Site 801. Bedrock isochrons are represented by magnetic anomaly lineations (29, 34, M0 and M17) on the Pacific plate [52]. The area inside the M17 isochron is underlain by Jurassic basement. The shaded areas represent the generalized outlines of oceanic plateaus, atolls and guyot groups in the western Pacific Ocean, as well as younger areas beyond the Pacific subduction zones.

represent an off-ridge-crest eruption that buried the hydrothermal zone of presumably intermediate age between the two different lava sequences. The recovered portions of the hydrothermal unit consist of highly altered alkali basalts overlying a yellow, iron- and silica-rich oxyhydroxide. Only 1 m of the altered alkali basalt was recovered in Core 129-801C-3R, and 3 m of the hydrothermal precipitate were recovered in Core 129-801C-4R. Some radiolarian ooze that was deposited on the Jurassic ridge crest may have been incorporated into the hydrothermal unit, but none was recovered. The 18 m thickness of this entire unit is somewhat greater than that supposed on Leg 129 [1], partially due to the inclusion of the altered alkali basalts at 510–515 mbsf, but this thickness is confirmed by large anomalies between 510 and 528 mbsf in all the logs shown in Fig. 2. These anomalies, and the geochemical logs [5] (not shown here), also suggest that the physical and chemical natures of the hydrothermal zone are quite variable, and that the recovered material may not be representative of the majority of the interval.

The upper alkali basalts have velocities, densities and resistivities that are all generally less than the lower tholeiitic basalts. Calculated porosities are generally higher in the alkali basalts than in the underlying tholeiitic basalts. In general, these logs are all of high quality, although the correction factors used for the density log within the hydrothermal zone suggest some uncertainty due to large variations in hole diameter, and the induction tool was often saturated by the highly resistive rocks of the tholeiitic basalts.

3. Introduction to permeability measurements

Prior to testing in Hole 801C, successful permeability measurements had been completed only in relatively young crust of the Costa Rica Rift at DSDP/ODP Hole 504B (5.9 Ma) [6–8], the Mid-Atlantic Ridge at DSDP/ODP Hole 395A (3.7 Ma) [9,10], the Southwest Indian Ridge at ODP Hole 735D (10–12 Ma) [11], and on the Juan de Fuca Ridge at ODP Holes 857D and 858G (< 0.2 Ma) [12]. Permeability is determined with controlled pressure variations in a portion of the drillhole that is physically isolated with an inflatable device called a drillstring packer. The

packer used during Leg 144 was resettable, and was incorporated into a special bottom-hole assembly (BHA) [13]. It was configured with a single element that, upon inflation, isolated the borehole below the packer element.

The packer is activated using a 'go-devil' that contains seals to redirect fluid pumped down the drill pipe to inflate the element and allow testing of the formation. The go-devil also contains a downhole gauge to record pressures in the isolated zone. When the element is inflated, it must form a good mechanical and hydraulic seal against the side of the borehole. Once the go-devil is dropped and in place inside the packer, fluid pumped down the drillpipe inflates the element. When the packer element begins to hold firmly against the borehole wall, 5000–10,000 kg of drillstring weight is transferred onto the packer. This weight shifts an inflation sleeve inside the packer, locking pressure in the element and opening up a passage through the packer into the borehole below. On Leg 144, fluid within the drillstring as well as the isolated zone was pressurized during testing, and a gauge at the rig floor was used to

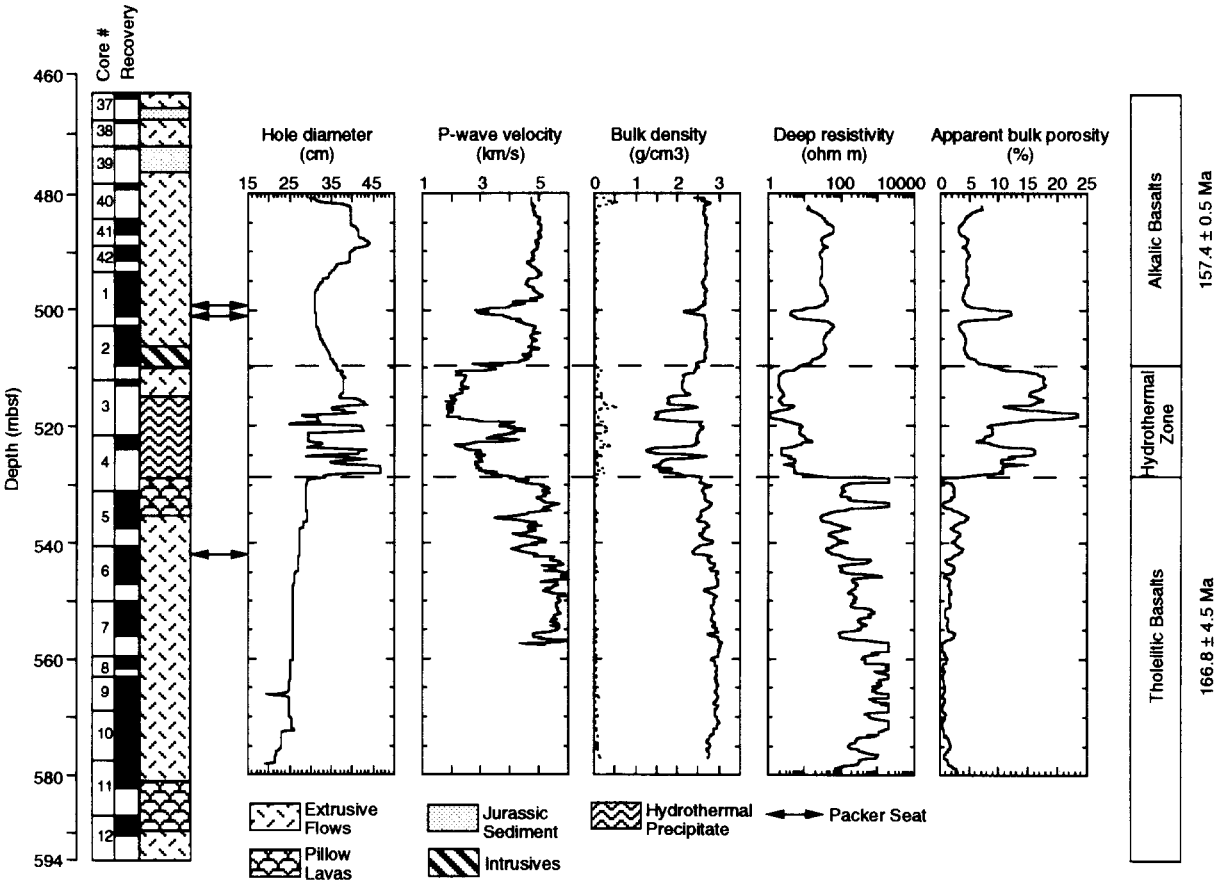

Fig. 2. Summary of coring and logging data from the upper basement at Site 801. Core data on the left-hand side of the diagram include sub-bottom depths, core numbers from Holes 801B (37-42) and 801C (1-12), recovery (black = recovered core, pushed to the top of each cored interval; white = unrecovered) and basement morphology (modified from [1]). The small, double-ended arrows next to the morphology column indicate packer seat levels used in Hole 801C during Leg 144. The central five curves illustrate results from logs run in Hole 801C during Leg 144. The caliper log is from the Formation MicroScanner string. The other data are from the geophysical string. The P-wave velocity log was processed to remove cycle skips and noise. The bulk density log includes a plot of the density correction (dashed line), which is an indication of log quality. The deep resistivity log was inverted using Archie's Law [53] with variables $a = 1$ and $m = 2$ [54], to yield apparent bulk porosity. Note the delineation of the hydrothermal zone. The column on the right-hand side of the figure indicates Ar/Ar ages determined for the alkali and tholeiitic basalts [4].

monitor and record pressures in real time (Figs. 3 and 4). The rig-floor gauge functioned well during Leg 144, which is fortunate as the downhole gauge failed.

There are two types of packer tests, pulse and injection. The pulse test [14–16] is best for formations having relatively low permeability. A pressure pulse of short duration is applied to the isolated zone; the shape of the pressure decay curve is then matched to a type curve. An injection test is used if the pressure from pulse tests decays very rapidly, the latter indicating that the formation is highly permeable. In the injection test, the isolated formation is subjected to continuous fluid pumping at a constant rate. The associated rate of pressure increase within the isolated zone, when plotted against log time, is proportional to permeability [17,18]. The pressure rise is analogous to the rise in temperature associated with thermal conductivity measurements [19,20]. After pumping is stopped and the hole is shut in, the subsequent pressure drop can be used independently to estimate permeability, with the method of analysis closely following that for injection testing.

Pressure test evaluation, as presented here, assumes that permeability is uniform and isotropic within the isolated zone. Particularly in crystalline rocks, where permeability is probably dominated by fractures, this assumption breaks down. The permeabilities calculated here are equivalent, or Darcian, porous-medium values; the actual hydraulic conductivities of individual fractures will certainly be higher than the calculated transmissivities. These bulk permeabilities are useful for comparative purposes, but as absolute values they should be viewed with some caution.

4. Leg 144 temperature and permeability experiments

Temperatures were recorded in Hole 801C with the LDEO self-contained temperature tool, which was attached to the bottom of the first logging string run into Hole 801C during Leg 144 [5]. Heat flow was determined using the Bullard [21] method of plotting individual temperatures versus cumulative thermal resistance, with thermal resistance determined at each temperature-measurement depth using thermal conductivity

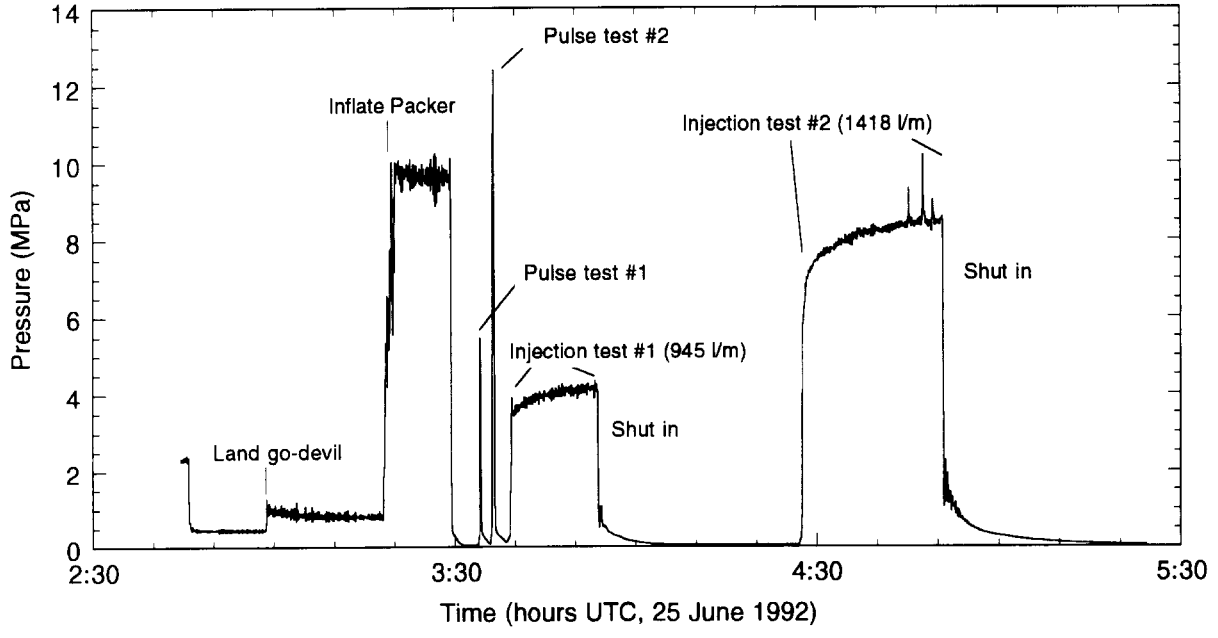

Fig. 3. A pressure–time record of the first packer tests at 501 mbsf in Hole 801C, measured with a gauge at the rig floor of the *JOIDES Resolution* during Leg 144. Pulse tests decay extremely rapidly, while injection tests display a gradual rise in pressure with time typical of a good packer seal and a permeable formation.

data from ODP Leg 129 [1]. The conductivity data were used to determine average conductivities for each lithology recovered at Site 801, and then coring and logging data from the sedimentary section of Hole 801B [22] were inverted to reconstruct the distribution of sedimentary layers and conductivities (Table 1). The resulting Bullard plot from Hole 801C shows no indication of significant fluid flow down the casing or into the formation from the borehole, and reveals conductive heat flow of approximately 52 mW/m^2 (Fig. 5). This heat flow is consistent with data from somewhat younger oceanic crust [23], and slightly higher than that predicted for crust of this age by either the 'uniform half space' or 'cooling plate' models of lithospheric cooling [e.g., 24,25], although it is closer to the latter.

The first packer seat in Hole 801C, selected on the basis of massive core recovery [1] and the caliper log, was at 501 mbsf, about 20 m below the bottom of the casing (Fig. 2). After the go-devil was prepared and dropped down the pipe, a slight but steady increase in drillpipe pressure monitored at the surface indicated that the go-devil had formed a good seal inside the packer (Fig. 3). The rig mud pumps were then used to

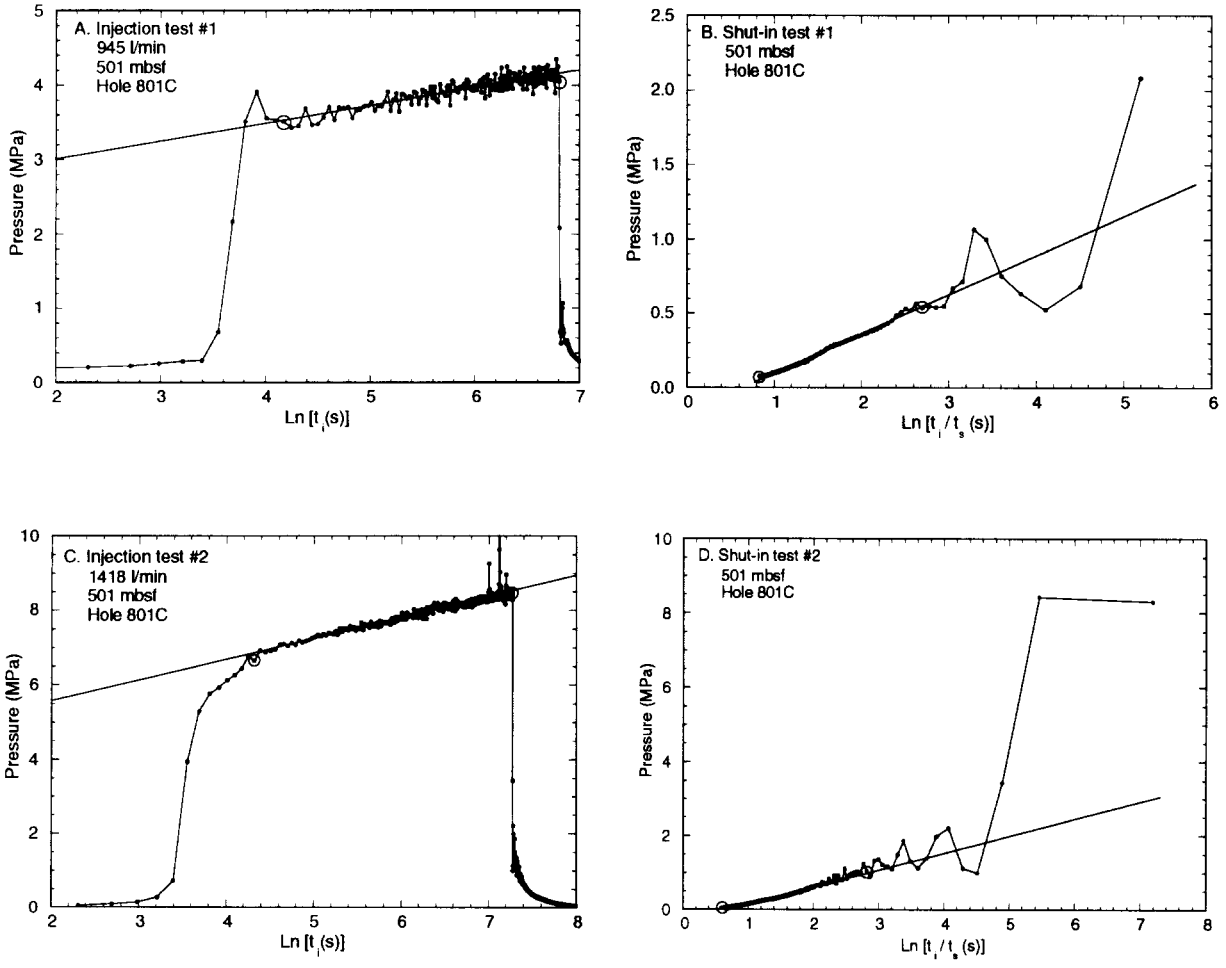

Fig. 4. Pressure–time records from the two injection and shut-in tests illustrated in Fig. 3 and used to estimate bulk permeability in Hole 801C. In each case the connected dots (•) are individual data points collected every 5 s. The straight lines are the least-squares, best-fits to the data values between the circles (○) on each plot. It is these portions of each dataset that are used for calculating the permeability values in Table 1. In all plots, t_i refers to the time since the start of injection, and t_s is the time since shut-in.

inflate the packer element to 10 MPa. A drill collar weight of 7500 kg was then applied to the packer, locking it inflated as the setting sleeve shifted. The packer held position steadily, but the pressure monitored at the rig floor dropped immediately from 10 to less than 0.5 MPa, indicating that the zone below the packer was highly permeable, or that the packer element was not forming a good hydraulic seal. Two additional pulse tests were conducted, and in both cases the pressure decay was rapid and immediate.

The first injection test was then started by continuous pumping at 945 l/min, and pressure jumped initially to 3.4 MPa, then gradually approaching 4.2 MPa (Fig. 3). Pumping was continued for 15 min, and then the hole was shut in for 30 min. A second injection test was conducted with a pumping rate of 1418 l/min for 24 min. Pressure jumped quickly to 5.0 MPa and then gradually approached 8.5 MPa. Pumping was stopped and the hole was shut in again. To check for the possibility of a leaky packer seal, the packer was deflated, raised 2 m in the hole and reset at 499 mbsf (Fig. 2). The element was again inflated to 10 MPa, and two pulse tests again decayed almost immediately. Analysis of injection test data for the first seat (below) shows good straight-line fits to the pressure increase and decay data when displayed as a function of log time, in accord with the theory of radial flow away

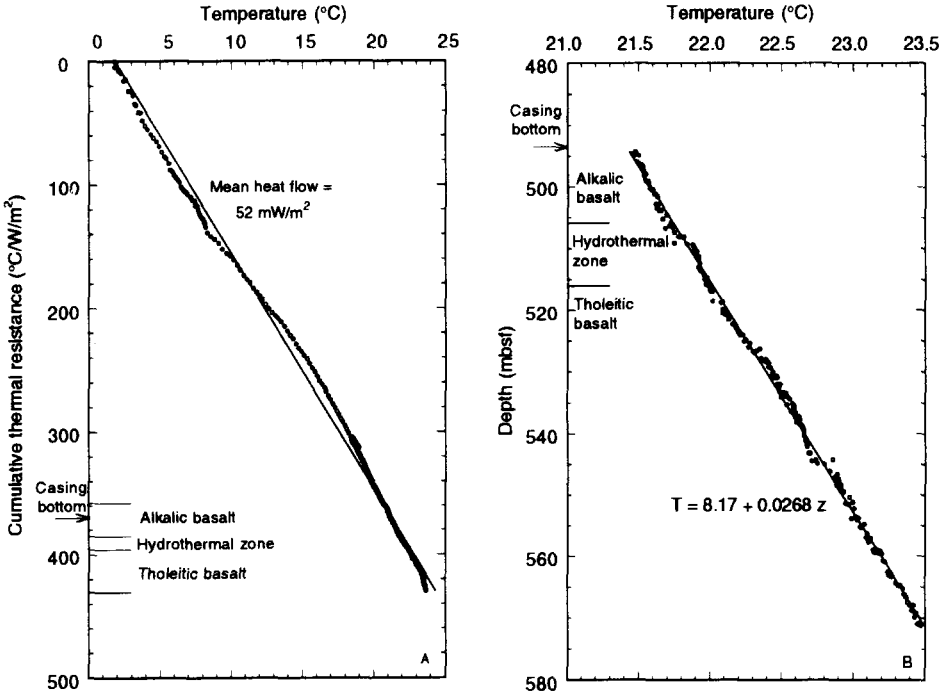

Fig. 5. (A) Bullard [21] plot of temperature versus cumulative thermal resistance in Hole 801C. Temperature data were collected with the self-contained, LDEO temperature logging tool, which was attached to the bottom of the first logging string run into Hole 801C upon re-entry during Leg 144. This tool records temperature versus time; times are later assigned to depths from the standard logging records. Thermal resistance was calculated from thermal conductivity measurements made on samples from Holes 801B and 801C [1]. The straight line is the least-squares best-fit to the data. Boundaries between the various basement units are shown, as is the depth of the casing bottom of the drillpipe. The hole below the drillpipe casing is open. Heat flow appears to be dominantly conductive, through both the cased interval and open hole. The broad deviations from a perfect linear fit probably reflect errors in the estimates of thermal conductivity. More local perturbations in the profile are probably due to errors in the calculated depths of each temperature measurement, perhaps because of changes in winch speed or ship heave. (B) Plot of temperature versus depth in the open basement section of Hole 801C. The good least-squares fit of the data to the line shown illustrates that (1) heat flow within the borehole is dominantly conductive, and (2) average thermal conductivity is relatively constant through this interval. A slight reduction in thermal gradient near 505 mbsf may reflect an increase in thermal conductivity, as documented for samples from the hydrothermal zone tested during Leg 129 [1].

TABLE 1

Thermal conductivities [a] used to calculate heat flow around Hole 801C

Interval [b] (mbsf)	Value [c] (W/m °C)
0–63.8	0.97
63.8–126.5	1.16
126.5–318.3	1.35
318.3–461.6	1.49
461.6–510.0	1.74
> 510.0	1.89

[a] Thermal conductivities for hand samples from Site 801 are reported in Shipboard Scientific Party [1].

[b] Depth intervals are from lithological boundaries defined by Shipboard Scientific Party [1].

[c] Thermal conductivities are mean values for samples within the first, third, fifth and sixth depth intervals, and a weighted mean of components within the second and fourth intervals, based on inferred lithological distributions from wireline logs in Hole 801B [22].

from a cylindrical pressure source. This suggests that the first packer seal was sound hydraulically as well as mechanically, although the seat was nearly coincident with a local anomaly in the density and velocity logs.

The pipe then was lowered to place the packer element at 542 mbsf, within the tholeiitic basalts below the hydrothermal zone, the go-devil was dropped, and packer inflation was attempted. The element was pressurized to about 8 MPa, which caused weight to be lost at the BHA and the drillstring to move about 3 m upward in the hole. The pumps were turned off and the element was allowed to deflate; then inflation was attempted twice again, each time with the same 'jack-up' result. The packer element would not maintain pressure when pumping was stopped, and the element would not support weight, indicating that a packer seal or the element was leaking. The drillpipe was raised back to 500 mbsf, where the earlier sets had been successful, and inflation was attempted again. Here the drillpipe was not jacked up the hole when inflation was attempted, but the element would, again, not support weight when pumping stopped. When the BHA was retrieved, the packer element was found to be ruptured in several places near the bottom.

5. Interpretation and discussion of permeability and temperature experiments

We interpret these events to indicate that the first two packer sets near 500 mbsf were successful, forming good mechanical and hydraulic seals,

TABLE 2

Summary of interval transmissivities and permeabilities in Hole 801C

Interval [a] (mbsf)	Test [b]	Flow rate [c] (l/min)	Permeability (m^2)	Transmissivity (m^2/s)
501–594	Inject 1	945	9.8×10^{-14}	5.2×10^{-4}
	Shut-in 1	–	9.2×10^{-14}	4.9×10^{-4}
	Inject 2	1418	6.4×10^{-14}	3.4×10^{-4}
	Shut-in 2	–	8.2×10^{-14}	4.1×10^{-4}
		mean:	8.4×10^{-14}	
		s.d.:	1.5×10^{-14}	
510–528	Inject 1	945	5.0×10^{-13}	5.2×10^{-4}
	Shut-in 1	–	4.8×10^{-13}	4.9×10^{-4}
	Inject 2	1418	3.2×10^{-13}	3.4×10^{-4}
	Shut-in 2	–	4.2×10^{-13}	4.1×10^{-4}
		mean:	4.4×10^{-13}	
		s.d.:	7.6×10^{-14}	

[a] The interval 501–594 mbsf is the entire isolated section of the borehole. The interval 510–528 mbsf only includes the limits of the hydrothermal zone, as determined from wireline logs. We prefer the second interpretation.

[b] There are four independent permeability measurements, two injection tests and two shut-in tests. Data are plotted in Figs. 3 and 4.

[c] The flow rate (for injection tests only) was determined from a gauge for the mud pumps in the driller's shack on the rig floor. The gauge shows the flow rate in strokes per minute, where one stroke = 18.9 l.

and revealing high permeability below this depth. The packer element was probably ruptured (perhaps by a ledge or projection in the hole) when it was lowered to the deeper part of the hole. Although the torn element would not hold pressure during setting attempts at 542 mbsf when the pumps were turned off, the loss of BHA weight and subsequent movement of the drillstring up the hole during inflation indicates that the formation below 542 mbsf is highly impermeable. This is supported by the geophysical logging information (Fig. 2). The inflation pressure leaked out from the bottom of the ruptured element, which had begun to seal against the borehole wall, and the resulting increase in pressure in the hole below pushed the drillstring upward like a piston. Because the element could not maintain inflation, the hydraulic seal with the borehole wall was immediately broken, allowing pressure to escape up the annulus. This hypothesis is consistent with the final attempted sets at 500 mbsf where the drillstring was not pistoned up the hole during attempted sets, because the permeable, hydrothermal zone now below the packer accepted the pulse of fluid released through the ruptured element.

Figure 4 illustrates the sections of data from the two injection tests and associated shut-in periods at 501 mbsf that were used to calculate bulk permeability, with the results summarized in Table 2. We chose to fit data over ranges when pressures (1) had become reasonably stable after initiation or cessation of pumping, and (2) closely followed theoretical curves for pressure rise or decay. The shapes of the pressure–time curves for all four tests are consistent with pressure changes in a radial geometry—an indication of a good hydraulic seal between the packer element and the borehole wall. If the entire 93 m section of open hole below the packer is assumed to have uniform hydrogeological characteristics, the mean calculated permeability from all four tests is 8.4×10^{-14} m^2 (standard deviation = 1.5×10^{-14} m^2). The geophysical logs (Fig. 2) and the behavior of the drillstring during our attempts to set the packer with a ruptured element suggest instead that the highest permeability is associated with the hydrothermal zone from 510 to 528 mbsf. If permeability is confined solely to the 18 m thick hydrothermal zone, the permeability of that zone is 4.4×10^{-13} m^2 (standard deviation = 7.6×10^{-14} m^2).

We believe the pressure fluctuations that occurred briefly at the start of both shut-in periods may be a response to standing pressure waves in the drillpipe. Deviations from ideal curves of transient pressure near the start of the injection tests may be due to departures from the assumptions of an idealized flow geometry and a homogeneous permeability distribution close to the borehole wall. When data ranges were adjusted to include all of these other data, the resulting permeabilities were within 8–18% of the individual values reported in Table 2. Additional uncertainties are associated with the large temperature dependence of the fluid viscosity in the borehole and formation. We assumed a bottom-water temperature of 2°C [5] for the fluid being pumped into the formation. All bulk permeability measurements are subject to errors, but we believe the raw data and interpretations reported are similar in quality to those obtained with a drillstring packer at other deep-sea locations. The permeabilities reported here for the entire 93 m interval from 501 to 594 mbsf of Hole 801C are slightly greater than those derived with the same broad-zone assumptions for the upper basaltic sections of Holes 395A and 504B in 3.7 and 5.9 Ma old oceanic crust, respectively. If the permeability in Hole 801C is concentrated within the 18 m thick hydrothermal zone, that unit could be 5–10 times more permeable than the upper crustal sections of Holes 395A and 504B, although there is evidence indicating that permeability in these much younger holes is also concentrated in thin zones [26].

When Hole 504B was first opened into upper basement, cold seawater flowed down the hole and into the surrounding formation at a downhole rate of at least 90 m/h [27]. Seawater has been flowing down Hole 395A near the Mid-Atlantic Ridge for at least 10 yr since that hole first penetrated basement [30–32]. Similar downhole flow has been detected at numerous other DSDP and ODP holes drilled through relatively impermeable sediments and into permeable upper basement. These flows result from the combination of (1) the presence of a permeable zone within upper basement, and (2) the contrast in density of a cold hydrostatic column of seawater

on an open borehole, and the warmer, lighter pore fluids present in the surrounding formation at some distance from the hole. We made the following calculations to determine if our measured bulk permeability in Hole 801C is consistent with the observed thermal structure.

Assuming that a radial diffusion equation applies to pressures surrounding Hole 801C, the expected transient flow of water, Q, down the hole 896 days ($\sim$ 2.5 yr) after it was drilled can be calculated as (corrected from [27], after [18]):

$$Q = 8k\Delta PhI(x)/(\pi\mu) \quad (1)$$

where $I(x)$ is the integral of Jaeger and Clark [28], and the other values are explained and referenced in Table 3. We calculated the pressure difference, ΔP, between hot and cold hydrostatic gradients at the depth of the permeable zone as a function of differences in fluid density to be 12,400 Pa, using the measured heat flow in Hole 801C, and the relationships for fluid properties of Haar et al. [29]. Based on the above solution to the radial diffusion equation, we calculate that the downhole volume flux due to density differences in Hole 801C 896 days after the Leg 129 drilling program should be 3.1×10^{-5} m^3/s, or a downhole rate of about 4.5×10^{-4} m/s. This volume flux is too small to have a measurable effect on the conductive thermal gradient apparent in the borehole. The temperature log (Fig. 5) is compatible with this calculation, because significant flow down the hole is neither predicted by the calculation nor observed in the temperature log. Regional thermal gradients are too low to support a large enough density contrast between bottom seawater and formation fluids to drive such flow 2.5 yr after drilling, despite the presence of one or more highly permeable zones in the upper basement. Significant fluid flow down Hole 801C might have been detected immediately after the hole was drilled if temperature logs had been collected during Leg 129, although at that time it might have been difficult to separate the thermal effects resulting from fluid flow down the hole from the thermal disturbance due to drilling. Temperature logs collected just after drilling in Hole 801B reveal no indication of fluid flow down that hole during Leg 129. Hole 801B penetrated into the alkali basalts, but not down to the hydrothermal zone. This also suggests that the high permeability in the Hole 801C crustal section is mainly associated with the hydrothermal zone.

The discovery that Jurassic oceanic crust contains a zone with extremely high permeability is surprising. This result is inconsistent with all models of crustal evolution [e.g., 33–35], which predict a monotonic decrease in crustal porosity with age, with a constant low value reached within a few tens of millions of years. Although there is indirect evidence of significant crustal permeability out to perhaps 70–100 Ma, as indicated by off-axis heat flow anomalies thought to be a result of hydrothermal circulation [36–38], it has not been previously suggested that 150–170 Ma old crust could contain permeable zones.

TABLE 3

Definition of parameters used to calculate permeability and the expected flow of fluid in Hole 801C

Parameter	Value tested	Source
k, permeability of most permeable zone	4×10^{-13}–8×10^{-14} m^2	packer tests, Leg 144
r, hole radius	0.15 m	caliper log
h, thickness of the most permeable interval	20–100 m	geophysical logs, Leg 144 (Fig. 2)
t, time since penetration of most permeable zone	896 days	
ϕ, porosity of permeable zone	5–20%	geophysical logs
μ, fluid viscosity	1.8×10^{-3} Pa s	[51]
c, fluid compressibility	4.25×10^{-10} Pa^{-1}	[29]
γ, Euler's constant	0.572	
$I(x)$, integral term	0.205–0.235	[28]

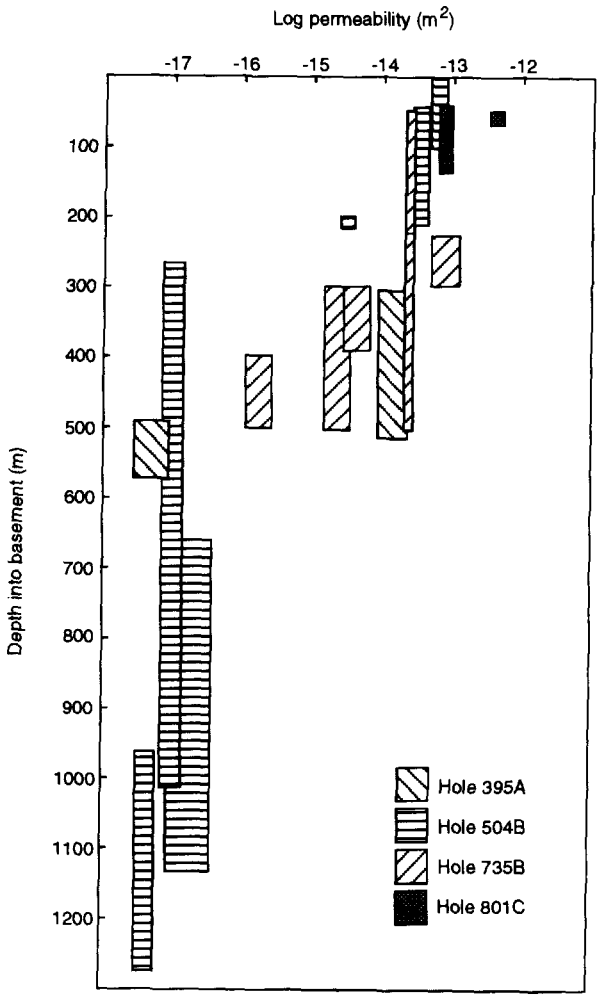

Fig. 6. Comparison of the permeability measured in the upper part of igneous basement in Hole 801C with previous results in much younger oceanic crust. Note that results are plotted against depth below the top of basement, rather than beneath the seafloor. Hole 395A was drilled in 3.7 Ma crust along the slow-spreading Mid-Atlantic Ridge [9,10], Hole 504B is in 5.9 Ma crust south of the moderate-spreading Costa Rica Rift [6–8], and Hole 735B is in a 10–12 Ma gabbroic section of the very-slow-spreading Southwest Indian Ridge [11]. While there appears to be a consistent trend with depth for the data overall, this result is probably in part fortuitous, as the data from Hole 735B are from a section of crust that probably originated at a much deeper structural level and has been 'unroofed' to its present depth.

A summary of permeability estimates in other DSDP and ODP upper crustal holes where packer measurements have been made is presented in Fig. 6. The permeability of the upper basaltic crust of Site 801 is clearly equal to, and possibly greater than, that of the other sites, despite the fact that the basaltic crust of Site 801 is at least 140 Ma older than that at the other sites. The relative representation in Fig. 6 may be somewhat misleading, because the small thickness of open crust in Hole 801C and it's highly layered structure made it possible to delineate an effective permeability along the narrow zone associated with the hydrothermal deposit. However, other upper crustal sections probably also have their permeability concentrated along narrow zones, as this characteristic is common in crystalline rocks, but packer testing thus far generally has not allowed detailed interpretation of the permeability structures in other oceanic settings. Recent developments with a spinner–flowmeter experiment conducted in conjunction with packer testing during the ODP [e.g., 39] eventually may provide a more detailed picture of the evolving permeability structure of upper oceanic crust as a function of both its depth and geological age.

It is likely that the highly permeable zone within Hole 801C is associated with the zone of hydrothermal sediment and basalt alteration that is present at the 4–14 Ma age discontinuity between the alkali and the tholeiitic basalts. However, we cannot determine if the permeable zone is associated with the deepest altered alkali basalts, the hydrothermal sedimentary rock, or both. Porosity was measured at 18.7% in these lowermost altered alkali basalts from Core 129-801C-3R, which is actually greater than the measured porosity of 8.0% in the iron- and silica-rich oxyhydroxide sedimentary rock from Core 129-801C-4R [1]. Neither can we determine the timing of hydrothermal activity relative to the emplacement of the overlying alkali basalts, but it is likely that the existence of these alkali basalts as a 'cap rock' has preserved the hydrothermal zone within the ocean crustal section.

Hydrothermal zones of this thickness have not been encountered in other ODP or DSDP drillholes into normal oceanic crust. While hydrothermal zones are fairly common in ophiolite sequences on land [40], they are usually confined to high-angle fault zones that have provided permeable pathways for hydrothermal solutions from below. These range in thickness up to a maximum of 1–2 m, so here again an 18 m thick hydrothermal zone would be a rarity. Nevertheless, Site 801

is located on what appeared to be normal oceanic crust on the basis of sea-surface measurements. Seismic velocities, heat flow, sediment cover, magnetic signature and depth to oceanic basement all fall within the broad ranges defining average values [41]. No massive faulting was observed in the underlying and overlying basalt samples, so there is no evidence that the hydrothermal zone is associated with faulting in the borehole, although an extensive underlying fracture and fault network must have existed somewhere in the vicinity to fuel the hydrothermal sediment deposit and basalt alteration. The hydrothermal zone is likely to be a pancake-shaped feature, mostly composed of chemical precipitate and highly altered basalts a few tens of meters thick and a few kilometers wide, resembling the hydrothermal zones forming at present-day centers of rapid seafloor spreading.

The key to understanding the generality of this result may be in estimating the frequency of off-axis volcanism, because an off-axis eruption probably preserved the highly permeable zone in Hole 801C. When this aspect of the problem is considered, it is possible, if not probable, that such highly permeable zones are common because off-axis volcanism due to mid-Cretaceous hotspots was common, especially beneath the western Pacific Ocean. More recent off-axis eruptions near Hawaii and Tahiti and other modern hotspots could continue the process at a reduced rate from 100 Ma to the present. Also, it has been recently reported [42–44] that extensive flood basalts and off-axis volcanism not associated with discrete hotspots are common near segments of the East Pacific Rise with spreading rates in excess of 10 cm/yr. Much of this off-axis volcanism is associated with seamounts situated on oceanic crust ranging in age from 2 to > 5 Ma [43]. This seems to be the most likely modern analog for the 801C situation, which formed at a spreading rate of 10–20 cm/yr, and where alkali basalts overlie the hydrothermal zone, and are 4–14 Ma younger than the underlying tholeiitic basalts. Floyd and Castillo [2] summarized the 801C basement lithostratigraphy as "typical of mid-ocean ridge basalt crust, generated at a spreading center, overlain by an off-axis seamount with ocean island basalt chemical characters".

It appears that a variety of types of off-axis volcanic products have 'overplated' normal oceanic crust in a number of areas, especially crust formed at fast spreading centers. This can potentially perturb the simple aging models [33–35] for normal oceanic crust in ways that may or may not be apparent, depending on the thickness of the off-axis overplating and its geometry. Much as seismic models of the oceanic crust have advanced from a layer-cake stratigraphy of discrete zones having constant velocities [45] to a varying number of diffusely bounded zones with different velocity gradients [46], so, too, realistic models of crustal architecture must now include off-axis, along-axis, and temporal variations in construction.

This architecture, including the presence of very permeable zones within the upper basement of even the oldest crust, has additional implications for several aspects of marine geology and geophysics. Off-axis hydrothermal systems within young crust may contribute to economically significant ore deposits [e.g., 47]. The global contribution of off-axis hydrothermal circulation to crustal and oceanic chemical balances of silica and magnesium may exceed the contribution from axial systems [48,49]. In addition, numerical simulations of off-axis hydrothermal systems suggest that chemically significant flow velocities may be maintained even with the minimum basal heat flow appropriate for the oldest oceanic crust, provided there is sufficient crustal permeability and some basement relief [50]. Even if communication between a permeable basement reservoir and the overlying ocean water is suppressed by the intervening sediments, circulation within the upper crust could potentially continue for many additional millions of years at low temperatures and low water/rock ratios, ultimately influencing the seismic, chemical and physical properties of the oldest remaining seafloor. These thin, permeable zones are likely to remain hidden to seismic surveys, particularly if they exist below thick sediment layers containing acoustically opaque volcaniclastics and chert. The seismic signature of these zones would probably be too small for detection with conventional, deep-water single- and multi-channel seismic equipment, as in the case at Site 801.

Site 801 provides our first, and so far only, direct glimpse of *in-situ* Jurassic oceanic crust

from the western Pacific, the last remnant of the Jurassic superocean. The lateral extent of the off-axis volcanic event that resulted in emplacement of the alkali basalts and the preservation of the hydrothermal sedimentary deposit are unknown. Off-axis volcanism is certainly common today, and was more common in the intervening geological record of the Cretaceous ocean basins. While the crustal and permeability structures detected at Site 801 may not fit easily into currently accepted models of crustal accretion and aging, these structures could actually be typical of large portions of the world's oceanic crust.

Acknowledgements

We thank Glen Foss, William Mills and Leon Holloway, who provided valuable advice and help during the permeability experiments. This work was supported by a grant from the NSF-JOI/U.S. Science Support Program to RLL. Acknowledgement is also made to the Donors of the Petroleum Research Fund, administered by the American Chemical Society, for partial support (to ATF) of this research.

References

1 Shipboard Scientific Party, Site 801, Proc. ODP, Init. Rep. 129, 91–161, 1990.
2 P.A. Floyd and P.R. Castillo, Geochemistry and petrogenesis of Jurassic ocean crust basalts, Site 801, Proc. ODP, Sci. Results 129, 361–388, 1992.
3 H.P. Johnson and R.L. Carlson, Variation of sea floor depth with age: A test of models based on drilling results, Geophys. Res. Lett. 19, 1971–1974, 1992.
4 M.S. Pringle, Radiometric ages of basaltic basement recovered at Sites 800, 801, and 802, ODP Leg 129, western Pacific Ocean, Proc. ODP, Sci. Results 129, 389–404, 1992.
5 Shipboard Scientific Party, Site 801, Proc. ODP, Init. Rep. 144, in press, 1993.
6 R.N. Anderson and M.D. Zoback, Permeability, underpressures and convection in the oceanic crust near the Costa Rica Rift, eastern equatorial Pacific, J. Geophys. Res. 87, 2860–2868, 1982.
7 R.N. Anderson, M.D. Zoback, S.H. Hickman and R.L. Newmark, Permeability versus depth in the upper oceanic crust: in-situ measurements in DSDP Hole 504B, eastern equatorial Pacific, J. Geophys. Res. 90, 3659–3669, 1985.
8 K. Becker, Measurements of the permeability of the sheeted dikes in Hole 504B, ODP Leg 111, Proc. ODP, Sci. Results 111, 317–325, 1989.
9 S.H. Hickman, M.G. Langseth and J.F. Spivack, In-situ permeability and pore pressure near the Mid-Atlantic Ridge, Deep Sea Drilling Project Hole 395A, Init. Rep. DSDP 78B, 699–708, 1984.
10 K. Becker, Measurements of the permeability of the upper oceanic crust at Hole 395A, ODP Leg 109, Proc. ODP, Sci. Results 106/109, 213–222, 1990a.
11 K. Becker, In-situ bulk permeability of oceanic gabbros in Hole 735B, ODP Leg 118, Proc. ODP, Sci. Results 118, 333–347, 1991.
12 Shipboard Scientific Party, Sites 857–858, Proc. ODP, Init Rep. 139, 283–569, 1992.
13 K. Becker, A guide to formation testing using ODP drillstring packers, ODP Tech. Note 10, 1990b.
14 H.H. Cooper, Jr., J.D. Bredehoeft and S.S. Papadopulos, Response of a finite diameter well to an instantaneous charge of water, Water Resour. Res. 3, 267–269, 1967.
15 S.S. Papadopulos, J.D. Bredehoeft and H.H. Cooper, Jr., On the analysis of 'slug test' data, Water Resour. Res. 9, 1087–1089, 1973.
16 J.D. Bredehoeft and S.S. Papadopulos, A method for determining the hydraulic properties of tight formations, Water Resour. Res. 16, 223–238, 1980.
17 D.R. Horner, Pressure build-up in wells, Proc. 3rd World Pet. Congr., II, p. 501, 1951.
18 C.S. Matthews and D.G. Russell, Pressure Buildup and Flow Tests in Wells (Soc. Pet. Eng. Monogr. 1), 1967.
19 J.C. Jaeger, The measurement of thermal conductivity and diffusivity with cylindrical probes, EOS 39, 708–710, 1958.
20 R.P. Von Herzen and A E. Maxwell, The measurement of thermal conductivity of deep-sea sediments by a needle-probe method, J. Geophys. Res. 64, 1557–1563, 1959.
21 E.C. Bullard, Heat flow in South Africa, Proc. R. Soc. London Ser. A173, 474–502, 1939.
22 A.T. Fisher, L. Abrams and W.H. Busch, Comparison of laboratory and logging data from Leg 129 and the inversion of logs to determine lithology, Proc. ODP, Sci. Results 129, 507–527, 1992.
23 J.G. Sclater, C. Jaupart and D. Galson, The heat flow through oceanic and continental crust and the heat loss of the earth, Rev. Geophys. Space Phys. 18, 269–311, 1980.
24 R.L. Parker and C.M. Oldenburg, Thermal models of ocean ridges, Nature 242, 137–139, 1973.
25 B. Parsons and D.P. McKenzie, Mantle convection and the thermal structure of the plates, J. Geophys. Res. 83, 4485–4496, 1978.
26 P.A. Pezard, Electrical properties of mid-ocean ridge basalt and implications for the structure of the upper oceanic crust in Hole 504B, J. Geophys. Res. 95, 9237–9264, 1990.
27 K. Becker, M. Langseth, R. Von Herzen and R. Anderson, Deep crustal geothermal measurements, Hole 504B, Costa Rica Rift, J. Geophys. Res. 88, 3447–3457, 1983.
28 J.C. Jaeger and M. Clarke, A short table of $I(0,1;x)$, R. Soc. Edinb. Proc. A61, 229–230, 1942.
29 L. Haar, J.S. Gallagher and G.S. Kell, NBS/NRC Steam Tables, 316 pp., Hemisphere, Washington, D.C., 1984.
30 K. Becker, M. Langseth and R.D. Hyndman, Temperature measurements in Hole 395A, Init. Rep. DSDP 78B, 689–698, 1984.

31 J. Kopietz, K. Becker and Y. Hamano, Temperature measurements at Site 395, ODP Leg 109, Proc. ODP, Sci. Results 106/109, 197–203, 1990.
32 R. Gable, R. Morin and K. Becker, Geothermal state of DSDP Holes 333A, 395A, and 534A: results from the Dianaut program, Geophys. Res. Lett. 19, 505–508, 1992.
33 R. Houtz and J.I. Ewing, Upper crustal structure as a function of plate age, J. Geophys. Res. 81, 2490–2498, 1976.
34 R.H. Wilkens, G.J. Fryer and J. Karsten, Evolution of porosity and seismic structure of upper oceanic crust: importance of aspect ratios, J. Geophys. Res. 96, 17981–17995, 1991.
35 R.S. Jacobson, Impact of crustal evolution on changes of the seismic properties of the uppermost oceanic crust, Rev. Geophys. 30, 23–42, 1992.
36 R.Anderson, M.G. Langseth and J. Sclater, The mechanisms of heat transfer through the floor of the Indian Ocean, J. Geophys. Res. 82, 3391–3409, 1977.
37 R. Embley, M. Hobart, R. Anderson and D. Abbott, Anomalous heat flow in the northwest Atlantic, a case for continued hydrothermal circulation in 80 MY crust, J. Geophys. Res. 88, 1067–1074, 1983.
38 M. Noel and M.W. Hounslow, Heat flow evidence for hydrothermal convection in Cretaceous crust of the Madeira Abyssal Plain, Earth. Planet. Sci. Lett. 90, 77–86, 1988.
39 K. Becker, R. Morin and E. Davis, Permeabilities in the Middle Valley hydrothermal system measured with packer and flowmeter experiments, Init. Rep. ODP 139, in press, 1993.
40 I.G. Gass and J.D. Smewing, Ophiolites: Obducted oceanic lithosphere, in: The Sea, Vol. 7, The Oceanic Lithosphere, C. Emiliani, ed., pp. 339–362, Interscience, New York, 1981.
41 L.J. Abrams, R.L. Larson, T.H. Shipley and Y. Lancelot, Cretaceous volcanic sequences and Jurassic crust in the East Mariana and Pigafetta Basins of the western Pacific, in: The Mesozoic Pacific, M. Pringle and W. Sager, eds., AGU Monogr., in press, 1993.
42 K.C. Macdonald, D.S. Scheirer, T. Atwater and D.W. Forsyth, Axial flood basalts are common on the southern East Pacific Rise where spreading rates exceed ~140 mm/yr, but rare at slower spreading rates. Why?, EOS 74, 297, 1993.
43 D.S. Scheirer, K.C. Macdonald, D. Forsyth and the Gloria Legs 2 and 3 Scientific Parties, An extensive seamount field near the southern East Pacific Rise, 15° to 19°S, EOS 74, 297, 1993.
44 M.R. Perfit, D.J. Fornari, S.J. Goldstein, R. Batiza and M.H. Edwards, Spatial and temporal variability of MORB across the East Pacific Rise at ~9°30′N: Implications for off-axis volcanism, EOS 74, 298, 1993.
45 R.W. Raitt, The crustal rocks, in: The Sea, Vol. 3, Ideas and Observations on Progress in the Study of the Seas, M.N. Hill, ed., pp. 85–102, Interscience, New York, 1963.
46 P. Spudich and J. Orcutt, A new look at the seismic velocity structure of the oceanic crust, Rev. Geophys. 18, 627–645, 1980.
47 U. Fehn, The evolution of low-temperature convection cells near spreading centers: A mechanism for the formation of the Galapagos Mounds and similar manganese deposits, Econ. Geol. 81, 1396–1407, 1986.
48 M.J. Mottl and C.G. Wheat, Hydrothermal circulation through mid-ocean ridge flanks: Fluxes of heat and magnesium, Geochim. Cosmochim. Acta, in press, 1993.
49 C.G. Wheat and R.E. McDuff, Geochemistry of dissolved silica in the Mariana Mounds, a mid-ocean ridge-flank hydrothermal system: Implications for global fluxes, Earth Planet. Sci. Lett., submitted.
50 A. Fisher, K. Becker and T.N. Narasimhan, Off-axis hydrothermal circulation: A refined model of DSDP/ODP Site 504 and parametric tests, J. Geophys. Res., submitted.
51 H.U. Sverdrup, M.W. Johnson and R.H. Fleming, The Oceans, Prentice Hall, Englewood Cliffs, N.J., 1942.
52 R.L. Larson, W.C. Pitman,III, X. Golovchenko, S.C. Cande, J.F. Dewey, W.F. Haxby and J.L. LaBrecque, The bedrock geology of the world, Freeman, New York, 1985 (one chart).
53 G.E. Archie, The electrical resistivity log as an aid in determining some reservoir characteristics, Pet. Trans. AIME 146, 54–62, 1942.
54 K. Becker, Large scale electrical resistivity and bulk porosity of the oceanic crust, Init. Rep. DSDP 83, 410–428, 1985.